Available online at www.sciencedirect.com

SCIENCE DIRECT®

Earth and Planetary Science Letters 236 (2005) 13–27

EPSL

www.elsevier.com/locate/epsl

Antipodal hotspots and bipolar catastrophes: Were oceanic large-body impacts the cause?

Jonathan T. Hagstrum*

U.S. Geological Survey, Menlo Park, California 94025, USA

Received 3 May 2004; received in revised form 13 December 2004; accepted 3 February 2005
Available online 23 June 2005
Editor: E. Boyle

Abstract

One aspect of the hotspot distribution that has received little attention is its antipodal character. Of 45 'primary' hotspots found in most hotspot compilations 22 (49%) form antipodal pairs within observed hotspot drift limits (≤ 20 mm/yr). In addition, the available ages, or possible age ranges, for both hotspots of an antipodal pair tend to be similar (≤ 10 Myr difference) or overlap. Monte Carlo simulations indicate that the antipodal primary hotspots' locations and ages are not due to chance at the > 99% confidence level ($p < 0.01$). All hotspot pairs include at least one oceanic hotspot, and these are consistently opposite those hotspots related to large igneous provinces (LIPs) and continental volcanism. A mechanism of formation is considered in which minor hotspot volcanism is induced at, and flood basalt volcanism is triggered by seismic energy focused antipodal to, oceanic large-body impact sites. Because continental impacts are expected to have lower seismic efficiencies, continents possibly acted as shields to the formation of antipodal hotspot pairs. Published numerical models indicate that large oceanic impacts (10-km-diameter bolide) generate megatsunami capable of altering coastal depositional environments on a global scale. Past impact-generated megatsunami, consequently, could have left widespread stratigraphic records, possibly misinterpreted as indicating large rapid changes in eustatic sea level, and widely disrupted continental and marine sediment reservoirs responsible for abrupt changes in the isotopic composition of seawater. Phanerozoic mass extinction events, therefore, might have resulted primarily from catastrophic megatsunami in a dominantly oceanic hemisphere and the near contemporaneous effusion of vast quantities of noxious gases from flood basalt eruptions in a dominantly continental one. Published by Elsevier B.V.

Keywords: hotspots; large igneous provinces; large-body impacts; antipodal focusing of seismic energy; global mass extinctions

1. Introduction

Hotspots are relatively small areas of volcanism scattered across Earth's surface [1,2] (Fig. 1). Generally defined as sites of intraplate volcanism or excessive volcanism along divergent plate boundaries

* Tel.: +1 650 329 4672; fax: +1 650 329 4664.
E-mail address: jhag@usgs.gov.

0012-821X/$ - see front matter. Published by Elsevier B.V.
doi:10.1016/j.epsl.2005.02.020

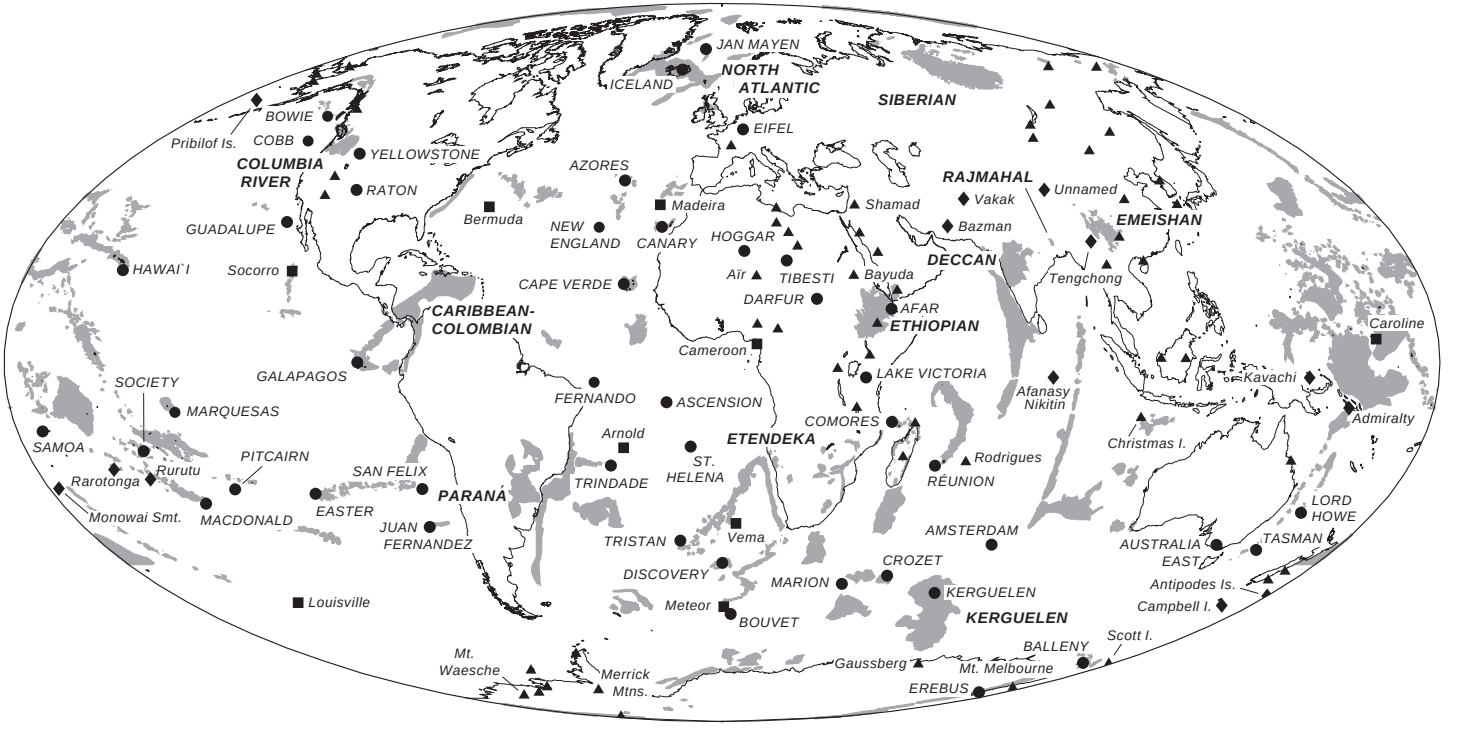

Fig. 1. World map showing locations of the primary hotspots (circles; see Table 1 in Appendix A), secondary hotspots (triangles, 1–55; squares, 56–64; diamonds, 65–77; see Table 2 in Appendix A), and large igneous provinces (gray areas, names in bold italic [27]).

unexplained by plate tectonic theory, hotspots originate from melting anomalies in the upper mantle. Some of the more prominent hotspots were initiated along with flood basalt volcanism and continental rifting [3]. A number of models have been suggested to explain the origin of hotspots including tensional cracking of the lithosphere [4], reactivated zones of weakness [5], and localized shear melting [6]. Over the past several decades, however, hotspots and their related large igneous provinces (LIPs) have most often been attributed to deep-mantle plumes [7].

During that time the 'standard' plume model of narrow upwellings from the core–mantle boundary has undergone an increasing number of modifications in response to incompatible observations [8], and more recently has been rejected altogether by some authors [9]. Those currently challenging the plume model prefer an alternate model in which hotspots were caused by plate-related stresses that fractured the lithosphere allowing melt to reach the surface from shallow heterogeneous sources [9]. In this model, melt volumes large enough to form LIPs could have been caused by secondary, edge-driven convection in the upper mantle [10]. Although many hotspots are presently associated with lithospheric fractures [9], there are still some aspects of hotspot origins (e.g., radial dike swarms, continental rifting) that appear more compatible with presumed uplift and attendant fracturing related to large plume-like events.

Debate is also ongoing concerning whether or not hotspots and LIPs were formed from large-body impacts. Numerical modeling by Jones et al. [11] indicate that decompressive melting of the upper mantle by crater excavation could have caused flood basalt volcanism for the largest impactors ($\geq$ 20 km diameters). Ivanov and Melosh [12], however, argue that such enormous impacts would have been too rare to explain the terrestrial record of LIPs. Furthermore, no evidence of contemporaneous impact has been found associated with continental LIPs, like, for example, tektite strewn fields found nearby young craters (Botsumtwi, Reis) and at much greater distances from older and larger impact structures (Chesapeake Bay, Popigai, Chicxulub). Although LIPs might initially conceal source craters and their proximal ejecta blankets [11], subsequent tectonism and erosion, like that exposing feeder dikes beneath the youngest Columbia River Basalt (~17 Ma), would make them much more likely to have been found.

A second impact-related model of hotspot and LIP formation has been suggested in which minor hotspot volcanism was generated at large-body impact sites and flood basalt volcanism was triggered antipodally by focused seismic energy [13,14]. This model has been challenged because impacts are generally considered seismically too inefficient [15], and the Deccan Traps of India were not antipodal to, and began erupting several Myr before, the end-Cretaceous Chicxulub impact in Mexico. In addition, no clear example of impact-induced volcanism, unrelated to melt sheets, has been confirmed at any known terrestrial crater. Matyska [16] noted, however, that hotspot distributions for both large and small data sets have angular symmetries with maxima at 180° rotations. Moreover, Rampino and Caldeira [17] showed that hotspots from three similar data sets occur significantly more often as nearly antipodal pairs than do artificial hotspots in large numbers of randomly generated distributions. This study was undertaken, therefore, to further examine and test the antipodal character of Earth's hotspot distribution, to evaluate a possible mechanism of antipodal hotspot formation, and to briefly explore the geological implications of such a mechanism of hotspot origins.

2. Methods

Because many isolated volcanic centers have questionable 'hotspot' origins (Fig. 1), a list of the most prominent or 'primary' hotspots, common to most published lists, was constructed (see Table 1 in Appendix A). These hotspots were assumed to have formed from the largest causal events, which are presumed to be the most readily discernible of all such events from the geologic record. Within this group, the greatest causal events were most likely those associated with initial flood basalt eruptions. Antipodal sites for the list of primary hotspots were determined from their present surface locations, as done previously [16,17], which assumes that each hotspot directly overlies its melting anomaly in the upper mantle. Of critical importance to defining antipodal hotspot pairs is the drift of individual

hotspots over time. Plate reconstructions have shown average drift rates of 10 to 20 mm/yr [18], and of 5 to 80 mm/yr [19] over the last 50 to 65 Myr, between the Hawaiian hotspot and those in the Atlantic and Indian Oceans. Similar results have been obtained for Pacific Ocean hotspots over the last 100 Myr using seamount ages and their locations on the Pacific plate [20].

Hotspots can be long-lived (> 100 Myr) leaving 'tracks' of volcanic edifices on the overriding plate [21]. Comparisons of initiation ages for antipodal hotspot pairs were made to determine whether or not they formed contemporaneously. Exact ages for hotspots, however, are often difficult to ascertain or are unknown, particularly for those oceanic hotspots where part of their track has been subducted. Usually, at least minimum ages are available for each hotspot of an antipodal pair so that general comparisons could be made. Finally, Monte Carlo simulations were run to determine whether or not the antipodal primary hotspot locations and their estimated ages could have occurred by chance.

2.1. Hotspot lists

There is no overall agreement on the number of hotspots, and different criteria have been used to assemble various lists. A comprehensive catalog of hotspots often cited is Burke and Wilson's [1] original list of 122 or a modification thereof [22,23]. Shorter lists include fewer hotspots, usually between 40 and 50, meeting a larger number of specific criteria. These generally include a long-lived track, initial flood basalt eruptions, a high buoyancy flux, high $^{3}He/^{4}He$ ratios, and anomalously low shear velocities in the underlying mantle. Only 9 out of 49 hotspots on Courtillot et al.'s list [24], however, meet three or more of these criteria, and their inferred cause is deep-mantle plumes. The association of high $^{3}He/^{4}He$ ratios with deep-mantle sources (7 of 9 'deep-origin' hotspots [24]) is controversial and alternatively could indicate a deficit of ^{4}He from shallow mantle sources containing low amounts of U and Th [25].

A number of studies have shown that the overall distribution of hotspots is non-random and that they tend to be dispersed over roughly half of Earth's surface area [23]. Moreover, although they occur on both continental and oceanic crust, hotspots are particularly common at or near divergent plate boundaries [26]. Ocean plateaus, like continental LIPs, also tended to form at or near spreading centers and usually at triple junctions [27].

Table 1
Large igneous provinces, related hotspots, and antipodal hotspots

Large igneous province	Age (Ma)	Related hotspot	Location		Antipodal hotspot	Age (Ma)	Location		Ang. dist. (°)	Drift (mm/yr)
			Lat. (°)	Lon. (°)			Lat. (°)	Lon. (°)		
Columbia River	~17–15	**Yellowstone**	44 N	249 E	**Kerguelen**	~29–24	49 S	69 E	175	~19
Ethiopian	~31–29	**Afar**	11 N	43 E	**Marquesas**	~36	10 S	222 E	179	~3
North Atlantic	~62–58	**Iceland**	65 N	343 E	**Balleny**	≥ 36	67 S	163 E	178	~4
Deccan	~67–64	**Réunion**	21 S	56 E	**Guadalupe**	> 25	19 N	249 E	174	~10
Madagascar	~90–84	**Marion**	47 S	38 E	**Bowie**	> 30	53 N	225 E	173	~9
Caribbean-Colombian	~90–87	**Galápagos**	0 N	269 E	Afanasy Nikitin	~80–73	3 S	83 E	173	~9
Kerguelen-Rajmahal	~115–86	**Amsterdam(?)**	38 S	78 E	**Raton**	?	36 N	256 E	177	~3
Paraná-Etendeka	~134–129	**Tristan**	37 S	348 E	Pacific Ocean(?)	na	na	na	na	na
	~40	**Mt. Erebus**	77 S	167 E	**Jan Mayen**	≤ 50	71 N	352 E	174	~17
	~65	**Canary**	28 N	344 E	**Lord Howe**	> 50	31 S	159 E	175	~9
	≥ 20	**Crozet**	45 S	51 E	**Cobb**	> 40	47 N	229 E	178	< 6
	≥ 60	**Azores**	38 N	332 E	**Tasman**	> 50	39 S	156 E	177	< 6
	> 50	**E. Australia**	38 S	143 E	**New England**	≥ 60	28 N	327 E	169	< 20
	> 100	**Hawai'i**	19 N	205 E	**Lake Victoria(?)**	?	3 S	36 E	161	< 26

Primary hotspots in bold type (see Table 1 in Appendix A) and secondary hotspots in regular type (see Table 2 in Appendix A). Age references (see Table 3 in Appendix A). Ang. dist., angular distance between hotspots; Drift, calculated drift rate from exact antipodality assuming that ages of both hotspots are identical to that of the initial flood basalt eruptions (top group) or to the best limiting age (bottom group); na, not available.

2.2. '*Primary*' *hotspots*

The 45 primary hotspots used in this investigation (see Table 1 in Appendix A; Fig. 1) are from the intersection of Vogt's [22,23] long list (117), a modification of Burke and Wilson's [1] original list, and five more recently published shorter lists [2,21,28–30]. Many of the primary hotspots have been active over the past 1 Myr [31], and comparisons with a compilation of active Holocene volcanoes [32] show that most (67%) were active during the last 10 kyr. The remaining hotspots on Vogt's list (1–55) and the five short lists (56–64) are considered 'secondary' hotspots (Fig. 1; see Table 2 in Appendix A). Seventeen hotspot locations from Vogt's original list, however, have been omitted because no volcanic feature could be identified. Also included in Fig. 1 are other young volcanic centers found opposite to some of the primary hotspots (65–77; see Table 2 in Appendix A). Comparing hotspot locations between all of the lists mentioned above often shows variations of 2° or more for a given hotspot location, and in some instances differences of as much as 5°.

Many of the initiation ages for the primary hotspots have been taken from other hotspot compilations (e.g., [30]) or from ages available in the literature. In some cases, variable initiation ages have been inferred for a given hotspot by a number of authors; in these cases the age selections used in this analysis are discussed in greater detail. LIPs clearly associated with a single hotspot track, however, are often the best-dated indicators of hotspot initiation. Such provinces, related hotspots, and age estimates are listed in Table 1.

3. Results

3.1. Antipodal hotspots

Seven of the eight primary hotspots, most clearly associated with young LIPs, have near-antipodal, mostly primary, hotspots that could initially have been exactly antipodal within relatively conservative drift limits (< 20 mm/yr; Table 1). Drift limits were calculated assuming contemporaneous antipodal origins at the time of the initial flood basalt eruptions. The antipodal comparisons are necessarily skewed towards those between younger hotspots, roughly < 100 my in age, because near antipodal relationships become less certain over time with the decline in hotspot activity and the inordinate expansion of antipodal limits, even assuming modest hotspot drift rates.

The Kerguelen hotspot has generally been associated with formation of the Kerguelen Plateau, Broken Ridge, Rajmahal Traps, and the Ninetyeast Ridge, beginning at ~115 Ma [33]. The tectonic history of the eastern Indian Ocean, however, is complex and other interpretations have been made. The Kerguelen hotspot is located ~175° from the Yellowstone hotspot (Table 1). $^{40}Ar/^{39}Ar$ dating of acid-leached groundmass separates from basalts of the Kerguelen archipelago, assumed to overlie the Kerguelen hotspot, give ages between ~29 and 24 Ma. These ages, however, are much younger than the age of rifting between the Kerguelen Plateau and Broken Ridge (~40 Ma) expected to have been recorded at the Kerguelen hotspot [34]. Moreover, formation of Ninetyeast Ridge (36–84 Ma) and the Rajmahal Traps (~115 Ma) by the Kerguelen hotspot (49°S, 69°E) requires that it was ~10° farther north during those times [35]. Offset magnetic anomalies across Ninetyeast Ridge indicate that it is a complex feature unlike other hotspot tracks, and it could have originated as a leaky transform fault [36]. It has also been suggested that the Amsterdam hotspot was involved in Ninetyeast Ridge volcanism [37]. In addition, if the Kerguelen hotspot (a zone of crustal weakness) was associated with the greater Kerguelen/Broken Ridge LIP, then its present location on a rifted portion of the Kerguelen Plateau away from the SW Indian Ridge is peculiar. Other LIP-related hotspots such as Iceland and Tristan da Cunha have remained at or near the spreading center (Fig. 1). Alternatively, plateau volcanism in the southern Indian Ocean at ~115 Ma might have started along with the Amsterdam hotspot (38°S, 78°E) which presently sits ~10° farther N on the SE Indian ridge. Antipodal to the Amsterdam hotspot is the Raton hotspot, also of uncertain age, in northern New Mexico (~177°; Table 1).

Several ages of initiation for the Marquesas hotspot are also possible. Islands of the Marquesas archipelago indicate a minimum age for hotspot volcanism of ~6 Ma [30]. Crough and Jarrard [38], however, interpret a topographic swell between the Marquesas

Islands and Line Islands as a continuation of the Marquesas hotspot track, thus increasing the track length back to ~40 Ma. In addition, an age of ~36 Ma has been obtained from seafloor samples near the intersection of the Line Islands (having non-progressive ages) and the Marquesas swell [39]. Although peak flood basalt volcanism at the antipodal Afar hotspot (~179°; Table 2) occurred between ~31 and 29 Ma, and was associated with opening of the southern Red Sea and Gulf of Aden [40], regional volcanism began earlier at ~38 Ma [41]. The main problem in determining hotspot ages is illustrated in Table 1; subduction has truncated many oceanic hotspot tracks so that only minimum age estimates can be made. In general, however, comparisons of the ages for many of the antipodal hotspot pairs in Table 1 show that they are similar within ≤ 10 Myr, or, for those with only minimum ages, that their possible age ranges overlap (see Fig. 1 in Appendix A).

Of the 45 primary hotspots, 22 form antipodal pairs (49%) within moderate drift limits (≤ 20 mm/yr; Table 1). The Hawaii–Lake Victoria pair is omitted from this tally due to the large minimum age of the Hawaiian hotspot and thus the high probability of antipodal coincidence. Comparisons between primary and secondary hotspots are continued elsewhere (see Table 3 in Appendix A). Only 4 of the 45 primary hotspots are without near-antipodal volcanic features, and antipodes for these 4 hotspots would have been located in the ancestral Pacific Ocean. Moreover, there are few contradictions between well-defined ages within all the pairs (≤ 10 Myr), and no flood basalt related hotspots are antipodal to one another. Other pairs show near antipodality with no other hotspots nearby (Galápagos–Afanasy Nikitin, > 2500 km; Cape Verde-Kavachi, > 1300 km; see Table 3 in Appendix A) lending further support to a singular causal relationship between at least some of the hotspot pairs. Certainly, a number of these antipodal locations and age correlations are coincidental, and such coincidences would be especially likely in antipodal areas of high hotspot density and long-term volcanism (e.g., Africa, Pacific Ocean).

Table 2
Primary hotspot distribution versus random test cases

Limit (°) (L_{MAX})	Primary pairs (N_P)	$p(L_{MAX})$	$p(L_{MAX})$ ages	$p(L_{MAX})$ > 20° lat.	$p(L_{MAX})$ > 20° lat.; ages
2.0	2	0.031	0.0141	0.068	0.033
3.0	4	0.002	0.0005	0.013	0.004
4.0	5	0.004	0.0006	0.008	0.002
5.0	6	0.003	0.0004	0.021	0.001
6.0	7	0.004	< 0.0001	0.023	0.002
7.0	7	0.018	0.0011	0.082	0.008
8.0	9	0.006	< 0.0001	0.038	0.002
9.0	10	0.004	0.0002	0.061	0.006
10.0	11	0.003	0.0003	0.030	0.005

See text for explanation; hotspot drift rates not taken into account. Ages indicate that the actual hotspot ages (assigned ± 10 Myr errors; see Fig. 1 in Appendix A) are included in the analysis; > 20° lat. indicates that the 45 randomly generated hotspots are limited to spherical caps with latitudes > 20°N and S, equivalent to two thirds of the Earth's surface area or roughly the area of the oceanic basins.

The antipodal hotspot comparisons are illustrated in Fig. 2 (see also Fig. 1), where antipodal locations of all hotspots are plotted (see Tables 1 and 2 in Appendix A). Note that relatively few hotspots project onto continental crust at their antipodes, particularly those presently situated on continental crust. The exceptions are two secondary hotspots in Borneo (35–36) and a few volcanic fields from eastern Asia that project onto South America. The antipodes of the Merrick Mtns. and Gaussberg hotspots in Antarctica fall in northern Russia and Canada near large impact structures, and are discussed in Section 4.2. The main concentration of continental hotspots in Africa [1], above the African 'superswell', projects onto the concentration of hotspots above the Pacific 'superswell' [24] (see Fig. 2 in Appendix A). All primary hotspots, initially on continental crust, have antipodal locations in an oceanic setting (Table 1), except the Raton hotspot. However, if the Raton hotspot is as old as ~115 Ma, then it would have originally formed in the ancestral Pacific Ocean and later been overridden by the North American plate. Furthermore, 'spotless' areas as defined by Vogt [23] are generally on continental crust or antipodal to it, except for the antipodal African and Pacific hotspot provinces (Figs. 1 and 2), respectively.

3.2. Monte Carlo simulations

Although the overall groupings of the African and Pacific hotspots are antipodal to one another, the question becomes whether or not the nearly antipodal pairing of individual hotspots within these groups and elsewhere (Table 1; see Table 3 in Appendix A) is a

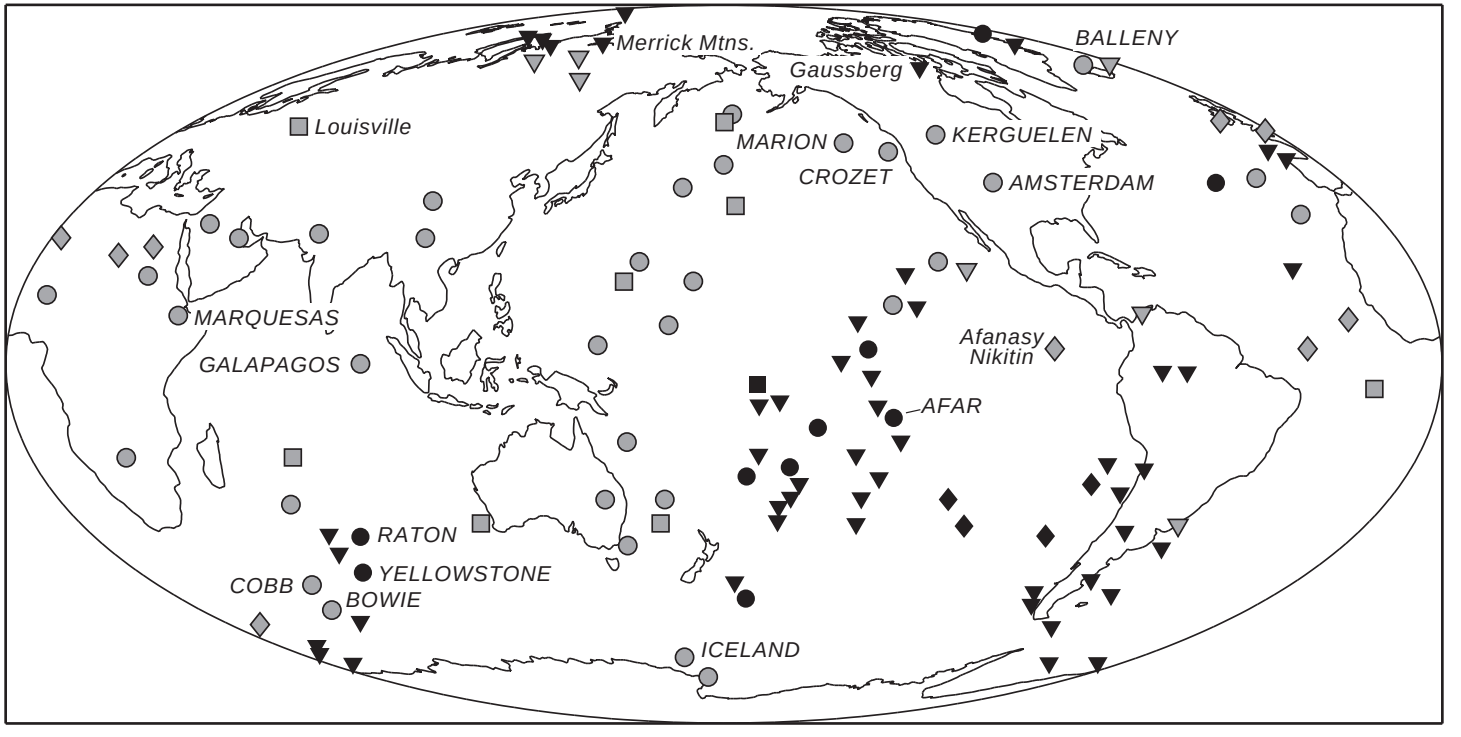

Fig. 2. Antipodal sites of all primary and secondary hotspots shown in Fig. 1. Black symbols indicate hotspots projected from locations on continental crust, and gray symbols indicated hotspots projected from locations on oceanic crust. Symbol shapes as in Fig. 1.

matter of chance. Rampino and Caldeira [17] tested the significance of antipodality for several published hotspot lists, within varying limits, by comparing them to large numbers (1000) of randomly generated distributions. A similar approach was adopted here to test for antipodal significance in the distribution of the 45 primary hotspots (Fig. 1), but with several notable modifications. Most importantly, in each random distribution an individual hotspot was assigned to only one other nearly antipodal hotspot within the set limit of antipodality (L_{MAX}). As L_{MAX} grows, an increasing number of individual hotspots from the artificial distributions have multiple near-antipodal hotspot pairs, but only the pair closest to exact antipodality was accepted. The number of primary hotspot pairs (N_P) within L_{MAX} values of 2.0° to 10.0° ranges from 2 to 11 and are listed in Table 2. Either 1000 or 10,000 random distributions of 45 hotspots were generated to test each null hypothesis, and for each L_{MAX} the fraction (p) of artificial distributions with at least as many antipodal pairs as the primary hotspot list (N_P) was determined.

Several null hypotheses concerning the primary hotspot distribution were examined (Table 2). In the first null hypothesis the primary hotspots were expected to be randomly distributed over the entire Earth's surface. For example, with L_{MAX} set to 10.0° only 3 randomly generated distributions out of 1000 have 11 (N_P) or more antipodal hotspot pairs ($p(L_{MAX})=0.003$). This null hypothesis, therefore, can be rejected for most L_{MAX} values at the > 99% ($p<0.01$) confidence level. A modification of this null hypothesis is that the actual age estimates for the primary hotspots (Table 1) are randomly associated with the artificially generated hotspots. Because of likely errors in the hotspot ages, point ages (e.g., ~90 Ma) were expanded to age ranges by ± 10 Myr error values (e.g., 80–100 Ma), and minimum ages (e.g., > 50 Ma) were expanded by a 10 Myr error value (e.g., 40–999 Ma; see Fig. 1 in Appendix A). Unknown ages were treated as wild cards (0–999 Ma) thereby matching any other hotspot age range. The assigned ± 10 Myr error ranges were more than enough to allow the age estimates of all antipodal pairs in Table 1 to overlap.

Again, the fraction (p) of random distributions with as many antipodal pairs as N_P, and with each artificial pair having overlapping age estimates, was calculated. This time it was necessary to generate 10,000 random distributions. For most L_{MAX} values the age-modified null hypothesis can be rejected at > 99.9% ($p<0.001$) confidence level (Table 2). Finally, similar null hypotheses were tested in which the artificial hotspot locations were limited to spherical caps (> 20° latitude) totaling two-thirds of the Earth's surface area or the approximate area of the oceanic basins. As will be discussed below, the area of the oceanic basins was selected because of expected differences between oceanic and continental impacts. Limiting the surface area is a more accurate and stringent test of the antipodal character of the primary hotspot distribution as it better represents the actual hotspot distribution and increases the chances of random antipodal alignment. Again, the null hypotheses of random distribution, and of random distribution with randomly assigned ages, for the spherical caps were tested. The null hypothesis without ages can be rejected for most L_{MAX} values at > 95% ($p<0.05$) confidence level, and, that with the ages included, mostly at > 99% confidence level ($p<0.01$; Table 2).

4. Discussion

4.1. Antipodal mechanism of hotspot formation

The Monte Carlo simulations presented in Section 3.2 indicate that the distribution of primary hotspots has a distinct antipodal character which is statistically significant at > 95% confidence level ($p<0.05$), and more tentatively, that the individual hotspot pairs formed contemporaneously. Possible explanations for the formation of antipodal hotspot pairs include (1) symmetries in mantle convection patterns and (2) mantle and lithospheric perturbations caused by the antipodal focusing of seismic energy from large-body impacts. The antipodal African and Pacific hotspot provinces might be explained by some type of long-term symmetry not yet recognized in models of mantle convection patterns (e.g., [42]). However, the near-exact antipodal alignment of widespread hotspot pairs (Table 1), each having similar or at least non-conflicting ages (see Fig. 1 and Table 3 in Appendix A), appears to refute such an explanation. Moreover, recent studies of Iceland [43] and

Yellowstone [44] provide strong evidence for shallow origins in the upper mantle further supporting the view of 'top-down' hotspot formation [8,9]. Although the antipodal effects of focused seismic energy from large-body impacts have been evaluated for a number of planetary bodies [45–47] application of this mechanism to Earth has been largely ignored.

Boslough et al. [14], however, used shock-hydrodynamic simulations to generate source functions for seismological modeling of the entire Earth, and estimated the effects of antipodally focused seismic waves from a Chicxulub scale impact (10-km-diameter asteroid impacting at 20 km/s). They found that the largest displacements (± 10 m at antipode), stresses, and strains occur in the antipodal lithosphere and upper asthenosphere, and that these large amplitudes are due primarily to the convergence of fundamental mode Rayleigh surface waves. Although peak stresses and strains fall off rapidly with depth beneath the antipode, the seismic energy remains sharply focused down to the core–mantle boundary. Indeed, motions at the core–mantle boundary are greater beneath the antipode than beneath the impact site itself.

Because the focused seismic energy would be most strongly attenuated in the partially molten asthenosphere, Boslough et al. [14] suggested that dissipation of the seismic energy could cause heating and additional melting, and possibly antipodal flood basalt volcanism. Ivanov and Melosh [48], however, concluded that the antipodal thermal anomaly generated by a Chicxulub scale impact would be negligible. Accepting that the upper mantle is likely hotter and more fertile than generally presumed in 'standard' mantle plume models [8,9], lithospheric fracturing by focused seismic energy from large-body impacts might have played a major role in the formation of antipodal flood basalts. As shown in Boslough et al. [14], peak antipodal displacements, stresses, and strains would occur throughout the lithosphere.

Low seismic velocities in the upper mantle above 300 km most likely indicate a zone of partial melting, and, because magmas are less dense than the overlying mantle and crust, volcanism could result from lithospheric cracking and melt focusing [9]. LIPs are related to large radial dike swarms [49], and Anderson [9] has calculated that relatively little strain (10^{-8}) would be needed over such areas (~1000 km across) to open cracks large enough (~1 cm) to produce flood basalt flow rates (~10^{-7} km^3/s). In most cases, the lack of uplift prior to flood basalt volcanism (e.g., [50]) also requires an explanation for the radial dike pattern other than mantle plumes or normal plate tectonic stresses. Melting anomalies in the upper mantle and antipodal hotspot pairs, therefore, might have been caused by crater excavation and decompressive melting at the impact site [11], and by more extensive lithospheric fracturing, initially producing flood basalt volcanism [9], concentrated at its antipode.

Impact-induced compressive waves within a planetary body reflect from its surface as convergent and opposing tensile waves. Numerical calculations for large basin-forming impacts on the Moon, Mercury, and Mars indicate that tensile stresses at and below the antipode would exceed the tensile strength of most common rock and could cause tensional fracturing to depths of tens of km [45–47]. The seismic energy (E_S) generated by an impact is generally assumed to be a small fraction of the total impact energy (E_T), because low seismic efficiencies ($E_S/E_T = 10^{-4}$) have been determined for nuclear explosions and lunar and terrestrial missile impacts [15]. Thus, it appears that large basin-forming impacts would be necessary to produce any significant antipodal effects. Because of the enormous dimensional differences between the documented impact and explosive events and past large-body impacts on Earth (e.g., ~10-km-diameter bolide), possibly much greater amounts of seismic energy would be produced from impacts penetrating deep into Earth's crust, and for oceanic impacts, well into the upper mantle [45,51]. Furthermore, shock wave attenuation is expected to be higher in continental crust due to hysteresis in the phase transitions of tectosilicates to denser phases, and, because of a steep release adiabat, faster rarefaction waves. Preliminary numerical modeling by De Carli et al. [52] of a 4-km-diameter asteroid impacting at 20 km/s indicate that significantly higher (~4 times) peak pressures occur in the mantle (32 km depth) for an oceanic impact than for a continental impact of similar scale.

It has been shown that most antipodal pairs of hotspots include at least one oceanic hotspot (see Table 3 in Appendix A), and that all LIPs and primary continental hotspots were initially opposite oceanic hotspots (Table 1; Fig. 2). Overall this result is not surprising because the Earth's surface has been divided

between primarily 'oceanic' and 'continental' hemispheres since at least mid-Paleozoic time. Because of low seismic efficiencies [15] and lack of volcanism associated with continental impact sites, and because oceanic impacts are potentially more seismically efficient [52], large oceanic impacts are inferred to have been responsible for the formation of antipodal hotspot pairs. Conversely, continents might have acted as shields to their formation. The known impact structures on Earth (see Fig. 3 in Appendix A) are all on continental crust with the exception of the recently discovered Ewing structure [53].

The relative lack of impact structures found on oceanic crust is largely due to subduction, as about half of the seafloor existing in the latest Cretaceous has subsequently been consumed. In addition, only a 4-km-diameter impactor is needed to excavate to the mantle beneath oceanic crust [52] versus a 10-km-diameter one for continental crust [51]. Moreover, submarine volcanic deposits possibly obscure the remaining large oceanic impact structures [11,51]. Oceanic large-body impacts (10-km-diameter asteroid) also differ from continental impacts in that the bulk of their high-velocity ejecta is water vapor containing only small amounts of crustal material [51], and that they generate megatsunami capable of widespread catastrophic effects [54]. Consequently, megatsunami are likely to have left coastal stratigraphic records of large oceanic impacts on a global scale [54].

4.2. Antipodes of terrestrial impact structures

Although the pattern of antipodal hotspot pairs suggests that continents acted as shields to the formation of antipodal hotspots, the idea needs further testing by examining the contemporaneous antipodes of large continental impact structures. In particular, does the shielding hold for even the largest impact energies? In order to evaluate this proposal, large (> 10 km), relatively young (< 100 Ma) and well-dated impact structures and their nearest antipodal hotspots (see Tables 1 and 2 in Appendix A) are determined (see Fig. 3 and Table 4 in Appendix A). Because impact structures move with the lithospheric plates, plate reconstructions are necessary to make initial antipodal comparisons. Both the change in crater location due to plate motions and in hotspot location due to drift are corrected for by transforming each location into African plate coordinates at the time of impact using the rotation poles compiled by Norton [55]. Again assuming exact initial antipodality, it should be noted that the calculated drift rates (see Table 4 in Appendix A) primarily reflect error in the plate and hotspot reconstructions because hotspot drift rates have already been taken into account.

After reconstruction, seven impact structures have nearly antipodal hotspots, generally low drift rates, and similar, or at least non-conflicting, age estimates (see Table 4 in Appendix A). The three largest impact structures (Chicxulub, Ewing, Popigai), all with diameters $\geq$ 100 km, apparently had contemporaneous, near antipodal volcanism. Unfortunately, no geochronologic data are available for the Merrick Mtns. in Antarctica (Fig. 1), although exposed volcanic rocks in the region are post early Oligocene in age [56] and are similar in maximum age to the age of the antipodal Popigai impact structure (~36 Ma). The drift rate for the Ewing-Comores antipodal pair is high (~69 mm/yr), but the pair's young age ($\geq$ 8 Ma) and perhaps an inexact location for the Comores hotspot ($\leq 5^{\circ}$) might contribute to the high rate. In this case, direct evidence of impact [53] has been found at an antipodal oceanic site. The Montagnais crater was nearly antipodal to the East Australian hotspot, as was the New England hotspot (Table 1), so at least one of these relationships is coincidental. The Louisville hotspot was nearly antipodal to the Boltysh crater at ~65 Ma and the Kamensk crater at ~49 Ma. Perhaps focused energy and antipodal lithospheric cracking from the second impact reinforced hotspot volcanism generated, or also reinforced, by the first. The cumulative eruptive volume of the Louisville chain shows a sharp increase near the 169°W bend in the chain (~47 Ma) due to the large 168.0°W volcano [57]. Both the Gaussberg hotspot in Antarctica and the Haughton crater in northern Canada have similar ages (~23–20 Ma) and were spatially nearly antipodal at that time. Moreover, the Gaussberg and Merrick Mtns. hotspots are two of the few continental hotspots with antipodal locations on continental crust (Fig. 2).

4.3. Implications of the impact-induced antipodal hotspot model

LIPs are characterized by enormous volumes of magma erupted within relatively short periods of time

[40]. Such high-volume eruptions are problematic, and McHone et al. [58] have suggested that lithospheric extension, magma ponding, diking and continental breakup preceded LIP eruption. Comparing age estimates for the youngest antipodal hotspot pairs in Table 1 indicates that volcanism at the oceanic (or 'impact') hotspots began ~5 Myr (Marquesas) and ≥ 7 Myr (Kerguelen) before eruption of the antipodal Afar and Columbia River LIPs, respectively. Regional volcanism also began several Myr before the Afar (~7 Myr [40,41]), North Atlantic (~5 Myr; [59]) and Deccan (~2–3 Myr [60]) LIPs were deposited. Thus, regional antipodal volcanism might have begun with lithospheric fracturing (radial dike swarms) as large magma reservoirs began to accumulate and pond within the upper mantle [58].

Subsequent rifting and massive basaltic eruptions might have followed as the fractured lithosphere responded to extensional plate tectonic forces. Impact-induced antipodal fracturing would likely have been influenced by lithospheric discontinuities, and could also have been antecedent to such linear volcanic features as Ninetyeast Ridge and the Cameroon Line. Hotspot volcanism at the impact site and its antipode might persist for an extended period of time as mantle material flows upward to replace that already withdrawn and erupted [11]. Due to differing characteristics of the impact site and underlying mantle [9], however, large oceanic craters (e.g., Ewing) might not be associated with long-term hotspot volcanism.

Global mass extinctions have also been associated with continental LIP events [61], as well as with large-body impacts, rapid regressive and transgressive changes in sea level [62], and abrupt changes in ocean chemistry [63]. Although the concurrence of these events at extinction boundaries, both in continental and marine settings, is generally considered coincidental, they might be related through the antipodal mechanism of impact-induced hotspot formation. The record of eustatic sea level change is based on interpretations of the depositional environments of shallow-water sedimentary sequences worldwide [64]. Synchronous increases in depositional energy on a global scale from impact-induced megatsunami would appear similar to, and could be misinterpreted as, eustatic sea-level falls. Sea level would then apparently rise as the depositional environments returned to their pre-megatsunami states.

The misinterpretation of depositional changes from impact-induced megatsunami could explain short-term regressive–transgressive pulses in sea level (see short-term curve in [64]), particularly those unrelated to climate cooling, and could also explain why such major oceanographic events have not been recognized in the stratigraphic record. Furthermore, due to their enormous size, depositional features related to megatsunami might locally appear unlike those related to smaller scale and more common earthquake- or landslide-induced tsunami events. Coeval shifts in ocean chemistry might also indicate disruption of continental and marine sediment reservoirs by megatsunami, like, for example, the introduction into the ocean of large quantities of ^{87}Sr-rich continental soils [65] and of ^{13}C-depleted carbon from disturbed methane gas hydrates [66], respectively.

The Cretaceous–Tertiary (K/T) Chicxulub impact was neither antipodal to nor coeval with initial Deccan volcanism on the Indian subcontinent. Antipodal to the Réunion hotspot, however, is the Guadalupe hotspot (Table 2) which at ~68–67 Ma would have been located in the northeastern part of the ancestral Pacific Ocean. Although oceanic crust in this region has been subducted and any potential crater destroyed, there is considerable evidence of profound environmental changes at ~68–67 Ma. At this time a large drop then rise in eustatic sea level [64], a distinct positive spike in the $^{87}Sr/^{86}Sr$ ratio of seawater [65], and extinctions of the rudistid clam reefs, inoceramid bivalves, belemnites, and shallow-water ammonite species [67] occurred. Climate change at ~68–67 Ma is also indicated by fossil records of the Hell Creek and other plant communities in the *Aquilapollenites* Province of western North America and Eastern Siberia [68]. In addition, a pre-K/T greenhouse episode of increased ocean temperatures [69] and elevated atmospheric CO_2 pressures [70] has been determined geochemically for this time from foraminifera ($\delta^{18}O$) and paleosol ($\delta^{13}C$) records, respectively. The K/T boundary impact, however, has been directly linked only to the rapid removal of many planktonic organisms [71] and to extinction of other species already in decline, and is viewed by many paleontologists as the coup de grâce of a global mass extinction already underway [67].

The Permian/Triassic (P/T) transition, the other era-ending catastrophe of the Phanerozoic, comprised two distinct events separated in time by ~5 Myr. The first pulse in extinction rates, perhaps as large as the K/T event, occurred at the end of the Kazanian stage, the penultimate stage of the Permian period [72]. At this time the Emeishan LIP of southern China (Fig. 1) was deposited [73] and eustatic sea level underwent apparent regressive and transgressive changes [74]. During the subsequent end-Permian event, an even greater mass extinction occurred as the Siberian Traps were erupted [75], and Holser and Magaritz [74] have inferred that sea level dropped, and then returned, by perhaps the largest amount in Phanerozoic time. For both the Siberian and Emeishan traps their antipodal sites during the P/T transition would have been on oceanic crust in the Southern Hemisphere. Thus, two large oceanic impacts close together in space and time might have triggered the end-Permian LIPs, and caused the apparent changes in sea level and shifts in ocean chemistry.

5. Conclusions

Models of hotspot (and LIP) origins are apparently in need of modification to explain the antipodal character of their distribution (Table 1). Herein, an inherently antipodal mechanism of hotspot formation is proposed in which one hotspot forms at an oceanic large-body impact site and a second hotspot and possible LIP are formed from seismic energy focused in the lithosphere and upper asthenosphere at the impact's antipode. Continental impact structures lack associated hotspot volcanism and are generally without antipodal volcanism, except for the largest ones that initially appear to have had small antipodal hotspots. Continents, due to their lower expected seismic efficiencies, therefore, are suggested to have mostly shielded the formation of antipodal hotspot pairs.

Only the Ewing impact structure has been identified on oceanic crust [53], and it is probable that other large oceanic craters have not been found because they are concealed by local impact-induced volcanism. Ejecta layers beyond the volcanic edifices of 'impact' hotspots like that from the Ewing crater could be identified, but would be much more difficult to find than ejecta layers from equivalent continental impacts because even large oceanic impacts eject mostly water or water vapor [51]. Material from the bolide itself would be difficult to find as well, because it makes up ≤ 1% of the total mass ejected from either a large continental or oceanic crater [51]. Large impacts are expected to produce widespread ejecta layers like that at the K/T boundary, which is distinctly visible in many sedimentary sections and deep-sea drill cores worldwide. The Ewing crater's ejecta layer, however, shows no visible change in drill cores from around the impact structure and was initially found using magnetic susceptibility measurements [53]. This method could also be used to find evidence of other oceanic impacts antipodal to continental hotspots and LIPs. Work is underway to find ejecta from the proposed 'Guadalupe' impact in deep-sea sediments that were deposited near the antipode of the Réunion hotspot and Deccan Traps at ~67–68 Ma [76].

Continued modeling of seismic efficiencies for large oceanic impacts using appropriate material models could also serve to test the antipodal focusing model [52]. The most prominent evidence of large oceanic impacts would probably be left in coastal stratigraphic records by megatsunami [54]. Phanerozoic global mass extinctions were associated with marked changes in apparent sea level and seawater composition [62,63], and both the P/T and K/T transitions possibly included multiple, primarily oceanic, large-body impact events. In light of the antipodal hotspot model, megatsunami might have ultimately been responsible for extinctions within the oceanic hemisphere [54] while vast quantities of noxious volcanic gases (CO_2, SO_2, HCl) were responsible for extinctions within the continental hemisphere [61]. Such bipolar catastrophes fit well with Raup's biogeographic analysis [77] that requires lethal areas to exceed a single hemisphere in order to generate global biologic crises.

Acknowledgements

Many thanks to D. Abbott, M. Boslough, E. Cecil, R. Christiansen, P. De Carli, L. Elkins-Tanton, J. Glen, S. Keiffer, K. Paddock, D. Roddy, and S. Ward for fruitful discussions, and to D. Abbott, E. Boyle, P.

De Carli, J. Glen, A. Glikson, S. Ingle, D. Jurdy, C. Klootwijk, B. Simonson, and P. Stoffer for constructive reviews of the manuscript. M. Coffin generously provided the map of LIPs used in Fig. 1.

Appendix A. Supplementary material

Supplementary data associated with this article can be found, in the online version, at doi:10.1016/j.epsl.2005.02.020.

References

[1] K.C. Burke, J.T. Wilson, Hot spots on the earth's surface, Sci. Am. 235 (1976) 46–57.
[2] S.T. Crough, D.M. Jurdy, Subducted lithosphere, hotspots, and the geoid, Earth Planet. Sci. Lett. 48 (1980) 15–22.
[3] B.C. Storey, T. Alabaster, R.J. Pankhurst, Magmatism and the causes of continental break-up, Geol. Soc. Spec. Pub., vol. 68, The Geological Society, London, 1992, 404 pp.
[4] D.L. Turcotte, E.R. Oxburgh, Mid-plate tectonics, Nature 244 (1973) 337–339.
[5] L.R. Sykes, Intraplate seismicity, reactivation of preexisting zones of weakness, alkaline magmatism and other tectonism post-dating continental fragmentation, Rev. Geophys. 16 (1978) 621–688.
[6] H.R. Shaw, E.D. Jackson, Linear island chains in the Pacific: results of thermal plumes or gravitational anchors? J. Geophys. Res. 78 (1973) 8634–8652.
[7] W.J. Morgan, Plate motions and deep mantle convection, Mem. Geol. Soc. Amer. 132 (1972) 7–22.
[8] www.mantleplumes.org.
[9] D.L. Anderson, The EDGES of the mantle, in: M. Gurnis, M.E. Wysession, E. Knittle, B.A. Buffett (Eds.), The Core–Mantle Boundary Region, Geodynamic Series, vol. 28, AGU, 1998, pp. 255–271.
[10] S.D. King, D.L. Anderson, Edge-driven convection, Earth Planet. Sci. Lett. 160 (1998) 289–296.
[11] A.P. Jones, G.D. Price, N.J. Price, P.S. DeCarli, R.A. Clegg, Impact induced melting and the development of large igneous provinces, Earth Planet. Sci. Lett. 202 (2002) 53–62.
[12] B.A. Ivanov, H.J. Melosh, Impacts do not initiate volcanic eruptions: eruptions close to the crater, Geology 31 (2003) 869–872.
[13] J.T. Hagstrum, B.D. Turrin, Is flood basalt volcanism a seismically-induced response to large antipodal bolide impacts? Eos Trans.-AGU 72 (1991) 516.
[14] M.B. Boslough, E.P. Chael, T.G. Trucano, D.A. Crawford, D.L. Campbell, Axial focusing of impact energy in Earth's interior: a possible link to flood basalts and hotspots, in: G. Ryder, D. Fastovsky, S. Gartner (Eds.), The Cretaceous–Tertiary Event and Other Catastrophes in Earth History, Spec. Pap.-Geol. Soc. Am., vol. 307, 1996, pp. 541–550.
[15] H.J. Melosh, Can impacts induce volcanic eruptions? Catastrophic events and mass extinctions: impacts and beyond, LPI Contrib. 1053 (2000) 141–142.
[16] C. Matyska, Angular symmetries of hotspot distributions, Earth Planet. Sci. Lett. 95 (1989) 334–340.
[17] M.R. Rampino, K. Caldeira, Antipodal hotspot pairs on the Earth, Geophys. Res. Lett. 19 (1992) 2011–2014.
[18] P. Molnar, J. Stock, Relative motions of hotspots in the Pacific, Atlantic and Indian Ocean since late Cretaceous time, Nature 327 (1987) 587–591.
[19] C.A. Raymond, J.M. Stock, S.C. Cande, Fast Paleogene motion of the Pacific hotspots from revised global plate circuit constraints, in: M.A. Richards, R.G. Gordon, R.D. van der Hilst (Eds.), The History and Dynamics of Global Plate Motions, Geophys. Monogr., vol. 121, AGU, 2000, pp. 359–375.
[20] A.A.P. Koppers, J.P. Morgan, J.W. Morgan, H. Staudigel, Testing the fixed hotspot hypothesis using $^{40}Ar/^{39}Ar$ age progressions along seamount trails, Earth Planet. Sci. Lett. 185 (2001) 237–252.
[21] M.A. Richards, B.H. Hager, N.H. Sleep, Dynamically supported geoid highs over hotspots: observation and theory, J. Geophys. Res. 92 (1988) 7690–7708.
[22] H.N. Pollack, I.G. Gass, R.S. Thorpe, D.S. Chapman, Reply to "comments on 'On the vulnerability of lithospheric plates to mid-plate volcanism: reply to P.R. Vogt' by H.N. Pollack, I.G. Gass, R.S. Thorpe, and D.S. Chapman", by M.A. Summerfield, J. Geophys. Res. 88 (1983) 1251–1254.
[23] P.R. Vogt, On the applicability of thermal conduction models to mid-plate volcanism: comments on a paper by Gass et al., J. Geophys. Res. 86 (1981) 950–960.
[24] V. Courtillot, A. Davaille, J. Besse, J. Stock, Three distinct types of hotspots in the Earth's mantle, Earth Planet. Sci. Lett. 205 (2003) 295–308.
[25] D.L. Anderson, The helium paradoxes, Proc. Natl. Acad. Sci. 95 (1998) 4822–4827.
[26] S.A. Weinstein, P.L. Olson, The proximity of hotspots to convergent and divergent plate boundaries, Geophys. Res. Lett. 16 (1989) 433–436.
[27] M.F. Coffin, O. Eldholm, Large igneous provinces, in: J.H. Steele, S.A. Thorpe, K.K. Turekian (Eds.), Encyclopedia of Ocean Sciences, Academic Press, London, 2001, pp. 1290–1298.
[28] N.H. Sleep, Hotspots and mantle plumes: some phenomenology, J. Geophys. Res. 95 (1990) 6715–6736.
[29] G.F. Davies, Ocean bathymetry and mantle convection: 1. Large-scale flow and hotspots, J. Geophys. Res. 93 (1988) 10467–10480.
[30] B. Steinberger, Plumes in a convecting mantle: models and observations for individual hotspots, J. Geophys. Res. 105 (2000) 11127–11152.
[31] V. Clouard, A. Bonneville, How many Pacific hotspots are fed by deep-mantle plumes? Geology 29 (2001) 695–698.
[32] T. Simkin, L. Seibert, Volcanoes of the World, 2nd ed., Geoscience Press, Inc., Tucson, AZ, 1994. 349 pp.

[33] D. Weis, F.A. Frey, A. Saunders, I. Gibson, Ninetyeast ridge (Indian Ocean): a 5000 km record of a Dupal mantle plume, Geology 19 (1991) 99–102.
[34] K. Nicolaysen, F.A. Frey, K.V. Hodges, D. Weis, A. Giret, $^{40}Ar/^{39}Ar$ geochronology of flood basalts from the Kerguelen Archipelago, southern Indian Ocean: implications for Cenozoic eruption rates of the Kerguelen plume, Earth Planet. Sci. Lett. 174 (2000) 313–328.
[35] C. O'Neill, D. Müller, B. Steinberger, Geodynamic implications of moving Indian Ocean hotspots, Earth Planet. Sci. Lett. 215 (2003) 151–168.
[36] J.G. Sclater, R.L. Fisher, Evolution of the east central Indian Ocean, with emphasis on the tectonic setting of the Ninetyeast ridge, Geol. Soc. Amer. Bull. 85 (1974) 683–702.
[37] K.T.M. Johnson, D.W. Graham, K.H. Rubin, K. Nicolaysen, D.S. Scheirer, D.W. Forsyth, E.T. Baker, L.M. Douglas-Priebe, Boomerang Seamount: the active expression of the Amsterdam-St. Paul hotspot, Southeast Indian Ridge, Earth Planet. Sci. Lett. 183 (2000) 245–259.
[38] S.T. Crough, R.D. Jarrard, The Marquesas-Line Swell, J. Geophys. Res. 86 (1981) 11763–11771.
[39] S.O. Schlanger, M.O. Garcia, B.H. Keating, J.J. Naughton, W.W. Sager, J.A. Haggerty, J.A. Philpotts, R.A. Duncan, Geology and geochronology of the Line Islands, J. Geophys. Res. 89 (1984) 11261–11272.
[40] R.E. Ernst, K.L. Buchan, Large mafic magmatic events through time and links to mantle-plume heads, in: R.E. Ernst, K.L. Buchan (Eds.), Mantle Plumes: Their Identification Through Time, Spec. Pap.-Geol. Soc. Am., vol. 352, 2001, pp. 483–575.
[41] J. Baker, L. Snee, M. Menzies, A brief Oligocene period of flood volcanism in Yemen: implications for the duration and rate of continental flood volcanism at the Afro-Arabian triple junction, Earth Planet. Sci. Lett. 138 (1996) 39–55.
[42] A. Yamaji, Periodic hotspot distribution and small-scale convection in the upper mantle, Earth Planet. Sci. Lett. 109 (1992) 107–116.
[43] G.R. Foulger, M.J. Pritchard, B.R. Julian, J.R. Evans, R.M. Allen, G. Nolet, W.J. Morgan, B.H. Bergsson, P. Erlendsson, S. Jakobsdottir, S. Ragnarsson, R. Stefansson, K. Vogfjord, Seismic tomography shows that upwelling beneath Iceland is confined to the upper mantle, Geophys. J. Int. 146 (2001) 504–530.
[44] R.L. Christiansen, G.R. Foulger, J.R. Evans, Upper mantle origin of the Yellowstone hotspot, Geol. Soc. Amer. Bull. 114 (2002) 1245–1256.
[45] P.H. Schultz, D.E. Gault, Seismic effects from major basin formation on the Moon and Mercury, Moon 12 (1975) 159–177.
[46] H.G. Hughes, F.N. App, T.R. McGetchin, Global seismic effects of basin-forming impacts, Phys. Earth Planet. Inter. 15 (1977) 251–263.
[47] D.A. Williams, R. Greeley, Assessment of antipodal-impact terrains on Mars, Icarus 110 (1994) 196–202.
[48] B.A. Ivanov, H.J. Melosh, Large scale impacts and triggered volcanism, Third International Conference on Large Meteorite Impacts, Nördlingen, Germany, 2003, (http://www.lpi.usra.edu/meetings/largeimpacts2003/pdf/4062.pdf).
[49] R.E. Ernst, K.L. Buchan, The use of mafic dike swarms in identifying and locating mantle plumes, in: R.E. Ernst, K.L. Buchan (Eds.), Mantle Plumes: Their Identification Through Time, Spec. Pap.-Geol. Soc. Am., vol. 352, 2001, pp. 247–265.
[50] G.K. Czamanske, A.B. Gurevitch, V. Fedorenko, O. Simonov, Demise of the Siberian plume: paleogeographic and paleotectonic reconstruction from the prevolcanic and volcanic record, north-central Siberia, Int. Geol. Rev. 40 (1998) 95–115.
[51] D.J. Roddy, S.H. Schuster, M. Rosenblatt, L.B. Grant, P.J. Hassig, K.N. Kreyenhagen, Computer simulations of large asteroid impacts into oceanic and continental sites—preliminary results on atmospheric, cratering, and ejecta dynamics, Int. J. Impact Eng. 5 (1987) 525–541.
[52] P.S. De Carli, A.P. Jones, G.D. Price, Continental vs. oceanic asteroid impacts, Abstr. Programs-Geol. Soc. Am. 36 (2004) 207.
[53] D.H. Abbott, A.A. Nunes, I.S. Leung, L. Burkle, J.T. Hagstrum, The Ewing impact structure: progress report, Eos Trans.-AGU 84 (2003) F977.
[54] T.J. Ahrens, J.D. O'Keefe, Impact of an asteroid or comet in the ocean and extinction of terrestrial life, J. Geophys. Res. 88 (1983) A799–A806.
[55] I.O. Norton, Global hotspot reference frames and plate motion, in: M.A. Richards, R.G. Gordon, R.D. van der Hilst (Eds.), The History and Dynamics of Global Plate Motions, Geophysical Mono., vol. 121, AGU, 2000, pp. 339–357.
[56] J.C. Behrendt, W. LeMasurier, A.K. Cooper, The West Antarctic rift system—a propagating rift "captured" by a mantle plume? in: Y. Yoshita, et al., (Eds.), Recent Progress in Antarctic Earth Science, Terra Sci. Pub. Co., Tokyo, 1992, pp. 315–322.
[57] P. Lonsdale, Geography and history of the Louisville hotspot chain in the southwestern Pacific, J. Geophys. Res. 93 (1988) 3078–3104.
[58] J.G. McHone, D.L. Anderson, Y.A. Fialko, Giant dikes: patterns and plate tectonics (http://www.mantleplumes.org/GiantDikePatterns.html).
[59] J. Skogseid, T. Pedersen, O. Eldholm, B.T. Larsen, Tectonism and magmatism during NE Atlantic continental breakup: the Vøring Margin, in: B.C. Storey, T. Alabaster, R.J. Pankhurst (Eds.), Magmatism and the Cause of Continental Break-up, Geol. Soc. Spec. Pub., vol. 68, 1992, pp. 305–320.
[60] A.R. Basu, P.R. Renne, D.K. DasGupta, F. Teichmann, R.J. Poreda, Early and late alkali igneous pulses and high-^{3}He plume origin for the Deccan flood basalts, Science 261 (1993) 902–906.
[61] P.B. Wignall, Large igneous provinces and mass extinctions, Earth-Sci. Rev. 53 (2001) 1–33.
[62] A. Hallam, P.B. Wignall, Mass extinctions and sea level changes, Earth-Sci. Rev. 48 (1999) 217–250.
[63] W.T. Holser, Catastrophic chemical events in the history of the ocean, Nature 267 (1977) 403–408.
[64] B.U. Haq, J. Hardenbol, P.R. Vail, Chronology of fluctuating sea levels since the Triassic, Science 235 (1987) 1156–1167.

[65] B.K. Nelson, G.K. MacLeod, P.D. Ward, Rapid change in strontium isotopic composition of seawater before the Cretaceous/Tertiary boundary, Nature 351 (1991) 644–647.
[66] M.E. Katz, D.K. Pak, G.R. Dickens, K.G. Miller, The source and fate of massive carbon input during the latest Paleocene thermal maximum, Science 286 (1999) 1531–1533.
[67] P.D. Ward, Rivers in Time, Columbia Univ. Press, New York, 2000, 315 pp.
[68] K.R. Johnson, L.J. Hickey, Megafloral change across the Cretaceous/Tertiary boundary in the northern Great Plains and Rocky Mountains, U.S.A., in: V.L. Sharpton, P.D. Ward (Eds.), Global Catastrophes in Earth History, Spec. Pap.-Geol. Soc. Am., vol. 247, 1990, pp. 433–444.
[69] E. Barrera, S.M. Savin, Evolution of late Campanian-Maastrichtian marine climates and oceans, in: E. Barrera, C.C. Johnson (Eds.), Evolution of the Cretaceous Ocean-Climate System, Spec. Pap.-Geol. Soc. Am., vol. 332, 1999, pp. 245–282.
[70] L. Nordt, S. Atchley, S. Dworkin, Terrestrial evidence for two greenhouse events in the latest Cretaceous, GSA Today 13 (2003) 4–9.
[71] J. Smit, W. Ten Kate, Trace element patterns at the Cretaceous–Tertiary boundary—consequences of a large impact, Cretac. Res. 3 (1982) 307–332.
[72] S.M. Stanley, X. Yang, A double mass extinction at the end of the Paleozoic era, Science 266 (1994) 1340–1344.
[73] K. Huang, N.D. Opdyke, Magnetostratigraphic investigations on an Emeishan basalt section in western Guizhou province, China, Earth Planet. Sci. Lett. 163 (1998) 1–14.
[74] W.T. Holser, M. Magaritz, Events near the Permian–Triassic boundary, Mod. Geol. 11 (1987) 155–180.
[75] P.R. Renne, Z. Zhang, M.A. Richards, M.T. Black, A.R. Basu, Synchrony and causal relations between Permian–Triassic boundary crises and Siberian flood volcanism, Science 269 (1995) 1413–1416.
[76] J.T. Hagstrum, D. Abbott, Evidence for a large bolide impact in the proto-Pacific Ocean preceding the Chicxulub impact by about 2 million years, Eos Trans.-AGU 83 (2002) F797.
[77] D.M. Raup, Biogeographic extinction: a feasibility test, in: L.T. Silver, P.H. Schultz (Eds.), Geological Implications of Impacts of Large Asteroids and Comets on the Earth, Spec. Pap.-Geol. Soc. Am., vol. 190, 1982, pp. 277–281.

Appendix A. Supplementary material

Table 1
'Primary' hotspot locations

Hotspot	Lat.(°)	Lon.(°)
1. **Afar** ***(Ethiopian)***	11 N	43 E
2. Amsterdam I.	38 S	78 E
3. Ascension[2]	8 S	346 E
4. Azores	38 N	332 E
5. Balleny Is.	67 S	163 E
6. Bouvet I.	54 S	3 E
7. Bowie Smt.[1]	53 N	225 E
8. Canary Is.	28 N	344 E
9. Cape Verde Is.	16 N	335 E
10. Cobb Smt.[1]	47 N	229 E
11. Comores	12 S	43 E
12. Crozet I.	45 S	51 E
13. Darfur	13 N	24 E
14. Discovery Smt.[1,2]	42 S	0 E
15. E. Australia	38 S	143 E
16. Easter I.	27 S	251 E
17. Eifel	50 N	7 E
18. Fernando Noronha[1]	4 S	328 E
19. **Galápagos Is.** ***(Caribbean-Colombian)***	0 N	269 E
20. Guadalupe I.	29 N	242 E
21. Hawai`i	19 N	205 E
22. Hoggar[1]	23 N	6 E
23. **Iceland** ***(North Atlantic)***	65 N	343 E
24. Jan Mayen	71 N	352 E
25. Juan Fernandez Is.	34 S	278 E
26. Kerguelen Is.	49 S	69 E
27. Lake Victoria	3 S	36 E
28. Lord Howe I.[1]	31 S	159 E
29. Macdonald Smt.	29 S	220 E
30. **Marion I.** ***(Madagascar)***	47 S	38 E
31. Marquesas Is.[1]	10 S	222 E
32. Mt. Erebus	77 S	167 E
33. New England Smt.[1]	28 N	327 E
34. Pitcairn I.[1]	26 S	230 E
35. Raton	36 N	256 E
36. **Réunion** ***(Deccan)***	21 S	56 E
37. St. Helena[1]	17 S	352 E
38. Samoa	14 S	187 E
39. San Felix	26 S	280 E
40. Society Is.	18 S	211 E
41. Tasman Smts.[1]	39 S	156 E
42. Tibesti	21 N	17 E

43. Trindade I.[2]	21 S	331 E
44. **Tristan da Cunha[2]** ***(Paraná-Etendeka)***	37 S	348 E
45. **Yellowstone** ***(Columbia River)***	44 N	249 E

Compiled from the intersection of Vogt's list [1] (as published by Pollock et al. [2]) with those of Sleep [3], Davies [4], Steinberger [5], Richards et al. [6], and Crough and Jurdy [7] (see Table 2 in Appendix A). Bold text indicates those hotspots most likely initiated by flood-basalt volcanism (bold-italic text; Table 1).

[1]No documented activity in the Holocene; see [8].
[2]No antipodal volcanic feature identified in the Pacific Ocean.

References

[1] P.R. Vogt, On the applicability of thermal conduction models to mid-plate volcanism: comments on a paper by Gass et al., J. Geophys. Res. 86 (1981) 950-960.

[2] H.N. Pollack, I.G. Gass, R.S. Thorpe, D.S. Chapman, Reply to "comments on 'On the vulnerability of lithospheric plates to mid-plate volcanism: Reply to P.R. Vogt' by H.N. Pollack, I.G. Gass, R.S. Thorpe, and D.S. Chapman", by M.A. Summerfield, J. Geophys. Res. 88 (1983) 1251-1254.

[3] N.H. Sleep, Hotspots and mantle plumes: some phenomenology, J. Geophys. Res. 95 (1990) 6715-6736.

[4] G.F. Davies, Ocean bathymetry and mantle convection, 1. Large-scale flow and hotspots, J. Geophys. Res. 93 (1988) 10467-10480.

[5] B. Steinberger, Plumes in a convecting mantle: models and observations for individual hotspots, J. Geophys. Res. 105 (2000) 11127-11152.

[6] M.A. Richards, B.H. Hager, N.H. Sleep, Dynamically supported geoid highs over hotspots: observation and theory, J. Geophys. Res. 92 (1988) 7690-7708.

[7] S.T. Crough, D.M. Jurdy, Subducted lithosphere, hotspots, and the geoid, Earth Planet. Sci. Lett. 48 (1980) 15-22.

[8] T. Simkin, L. Seibert, Volcanoes of the World, 2nd Ed., Geoscience Press, Inc., Tucson, AZ, 1994, 349 pp.

Appendix A. Supplementary material

Table 2
'Secondary' hotspot locations

Hotspot	Lat.(°)	Lon.(°)
1. Balagan-Tas *(Russia)*	66 N	144 E
2. Espenberg-Imuruk *(Alaska)*	66 N	196 E
3. Aluchin-Anjuisky *(Russia)*	66 N	165 E
4. Kookooligit Mtns. *(Alaska)*	64 N	190 E
5. Ingakslugwat Hills *(Alaska)*	62 N	196 E
6. Udokan *(Russia)*	56 N	118 E
7. Tseax River *(Canada)*	55 N	231 E
8. Dgida-Tunkin *(Russia)*	51 N	103 E
9. Wudalianchi *(China)*	49 N	126 E
10. Taryatu-Chulutu *(Mongolia)*	48 N	100 E
11. Chaine des Puys *(France)*	46 N	3 E
12. Dariganga *(Mongolia)*	45 N	114 E
13. Black Rock Desert *(Utah)*	39 N	247 E
14. Ch'uga-ryong *(Korea)*	38 N	127 E
15. San Francisco Peaks *(Arizona)*	35 N	248 E
16. Unnamed *(China)*[1]	34 N	113 E
17. Harrat as Shamad *(Syria)*	33 N	37 E
18. Halla *(Korea)*	33 N	127 E
19. Tripolitania *(Libya)*[1]	32 N	15 E
20. Jabal as Sawda *(Libya)*[1]	29 N	15 E
21. Haruj *(Libya)*	27 N	18 E
22. Harrat 'Uwayrid *(Saudi Arabia)*	27 N	37 E
23. Unnamed *(China)*[1]	26 N	106 E
24. Eghei *(Libya)*[1]	24 N	20 E
25. Harrat Kishb *(Saudi Arabia)*	23 N	41 E
26. Leizhou Bandao *(China)*	21 N	110 E
27. Ban Chiang Khian-Ban Hui Sai *(Thailand)*[1]	20 N	100 E
28. Bayuda *(Sudan)*	18 N	34 E
29. Aïr Massif *(Niger)*[1]	18 N	9 E
30. Jabal Haylan *(Yemen)*	15 N	45 E
31. Tullu Moje *(Ethiopia)*	8 N	39 E
32. Jos Plateau *(Nigeria)*[1]	8 N	9 E
33. Ngaoundéré (*Cameroon*)	7 N	14 E
34. The Barrier *(Kenya)*	2 N	37 E
35. Gunung Niyut *(Borneo)*[1]	1 N	110 E
36. Gunung Menyapa *(Borneo)*[1]	1 N	116 E
37. Nyamuragira *(Zaire)*	1 S	29 E
38. Kieyo *(Tanzania)*	9 S	34 E
39. Christmas I. *(Indian Ocean)*[1]	11 S	106 E
40. Ambre-Bobaomby *(Madagascar)*	12 S	49 E
41. Ankarata *(Madagascar)*	19 S	47 E
42. Rodrigues I. *(Indian Ocean)*	20 S	63 E

43. Mt. Abbot *(Australia)*[1]	20 S	148 E
44. Banks Peninsula *(New Zealand)*[1]	44 S	173 E
45. Dunedin Peninsula *(New Zealand)*[1]	46 S	171 E
46. Deception I. *(Antarctica)*	64 S	299 E
47. Gaussberg *(Antarctica)*[1]	67 S	89 E
48. Scott I. *(Antarctica)*[1]	68 S	180 E
49. Peter I. (*Antarctica*)	69 S	269 E
50. Hudson Mtns. (*Antarctica*)	74 S	261 E
51. Mt. Melbourne *(Antarctica)*	74 S	165 E
52. Merrick Mtns. *(Antarctica)*[1]	75 S	288 E
53. Mt. Takahe *(Antarctica)*	76 S	248 E
54. Mt. Waesche *(Antarctica)*	77 S	233 E
55. Mt. Early *(Antarctica)*[1]	87 S	206 E
56. Madeira Is. *(Atlantic Ocean)*[1]	33 N	343 E
57. Bermuda *(Atlantic Ocean)*[1]	33 N	293 E
58. Socorro I. *(Pacific Ocean)*	19 N	249 E
59. Caroline Is. *(Pacific Ocean)*[1]	5 N	164 E
60. Mt. Cameroon *(Cameroon)*	4 N	9 E
61. Arnold Smt. *(Atlantic Ocean)*[1]	17 S	335 E
62. Vema Smt. *(Atlantic Ocean)*[1]	33 S	4 E
63. Louisville Smt. *(Pacific Ocean)*[1]	51 S	219 E
64. Meteor Smt. *(Atlantic Ocean)*[1]	52 S	1 E
65. St. Paul I. *(Pribilof Is.)*	57 N	190 E
66. Unnamed *(W. China)*[1]	36 N	92 E
67. Vakak Group *(Afghanistan)*	34 N	68 E
68. Bazman-Taftan *(Iran)*	28 N	61 E
69. Tengchong *(S. China)*	25 N	98 E
70. Afanasy Nikitin Smt. *(Indian O.)*[1]	3 S	83 E
71. St. Andrew Strait *(Admiralty Is.)*	3 S	147 E
72. Kavachi *(Soloman Is.)*	9 S	158 E
73. Rarotonga *(Pacific Ocean)*[1]	22 S	201 E
74. Rurutu *(Pacific Ocean)*[1]	24 S	209 E
75. Monowai Smt. *(Kermadec Is.)*	26 S	183 E
76. Antipodes Is. *(Pacific Ocean)*	50 S	179 E
77. Campbell I. *(Pacific Ocean)*[1]	52 S	169 E

1-55, remainder of list from Vogt [1,2] (see Table 1 in Appendix A), and cross referenced with active volcanic centers of the world [3], Asia [4], the Antarctic plate [5], Africa [6] and New Zealand and Australia [7]. 56-64, hotspots left over from short lists [8-12] not found in long list. 64-77, antipodal volcanic features from various other sources considered in this study.

[1]No documented activity in the Holocene [3].

References

[1] H.N. Pollack, I.G. Gass, R.S. Thorpe, D.S. Chapman, Reply to "comments on 'On the vulnerability of lithospheric plates to mid-plate volcanism: Reply to P.R. Vogt' by H.N. Pollack, I.G. Gass, R.S. Thorpe, and D.S. Chapman", by M.A. Summerfield, J. Geophys. Res. 88 (1983) 1251-1254.

[2] P.R. Vogt, On the applicability of thermal conduction models to mid-plate volcanism: comments on a paper by Gass et al., J. Geophys. Res. 86 (1981) 950-960.
[3] T. Simkin, L. Seibert, Volcanoes of the World, 2nd Ed., Geoscience Press, Inc., Tucson, AZ, 1994, 349 pp.
[4] J.L. Whitford-Stark, A Survey of Cenozoic Volcanism on Mainland Asia, Geol. Soc. Am., Spec. Pap. 213, 1987, 74 pp.
[5] W.E. LeMasurier, J.W. Thomson (Eds.), Volcanoes of the Antarctic Plate and Southern Oceans, Am. Geophys. Union, Ant. Res. Ser. 48 (1990) 487 pp.
[6] M. Wilson, R. Guiraud, Late Permian to Recent magmatic activity on the African-Arabian margin of Tethys, in: D.S. Macgregor, R.T.J. Moody, D.D. Clark-Lowes (Eds.), Petroleum Geology of North Africa, Geological Society Spec. Pup. 132, 1998, pp. 231-263.
[7] R.W. Johnson, J. Knutson, S.R. Taylor (Eds.), Intraplate Volcanism in Eastern Australia and New Zealand, Cambridge Univ. Press, 1989, 408 pp.
[8] N.H. Sleep, Hotspots and mantle plumes: some phenomenology, J. Geophys. Res. 95 (1990) 6715-6736.
[9] G.F. Davies, Ocean bathymetry and mantle convection, 1. Large-scale flow and hotspots, J. Geophys. Res. 93 (1988) 10467-10480.
[10] B. Steinberger, Plumes in a convecting mantle: models and observations for individual hotspots, J. Geophys. Res. 105 (2000) 11127-11152.
[11] M.A. Richards, B.H. Hager, N.H. Sleep, Dynamically supported geoid highs over hotspots: observation and theory, J. Geophys. Res. 92 (1988) 7690-7708.
[12] S.T. Crough, D.M. Jurdy, Subducted lithosphere, hotspots, and the geoid, Earth Planet. Sci. Lett. 48 (1980) 15-22.

Appendix A. Supplementary material

Table 3

Near-antipodal hotspots on Earth

Oceanic site	Location Lat.(°)	Lon.(°)	Age (Ma)	Antipodal site	Location Lat.(°)	Lon.(°)	Age (Ma)	Ang. Dist.(°)	Drift ($^{mm}/_{yr}$)	Distance to next htspt (km)
Kerguelen	49 S	69 E	~29-24[1]	**Yellowstone**	44 N	249 E	~17[2]	175	~19	1440 / 560
Marquesas	10 S	222 E	~36[3,4]	**Afar**	11 N	43 E	~31[2]	179	~3	1440 / 440
Jan Mayen	71 N	352 E	≤50[5]	**Mt. Erebus**	77 S	167 E	~40[6]	174	~17	780 / 330
Balleny	67 S	163 E	≥36[7]	**Iceland**	65 N	343 E	~62[2]	178	~4	780 / 780
Lord Howe	31 S	159 E	>50[8]	**Canary**	28 N	344 E	~65[8]	175	~9	890 / 560
Guadalupe	29 N	242 E	>25[8]	**Réunion**	21 S	56 E	~67[8]	170	~10	890 / 780
Cobb	47 N	229 E	>40[8]	**Crozet**	45 S	51 E	≥20[9]	178	<6	780 / 1000
Tasman	39 S	156 E	>50[8]	**Azores**	38 N	332 E	≥60[9]	177	<6	890 / 1110
New England	28 N	327 E	≥60[9]	**E. Australia**	38 S	143 E	>50[8]	169	<20	1220 / 1110
Bowie	53 N	225 E	>30[8]	**Marion**	47 S	38 E	~90[2]	173	~9	440 / 1000
Raton	36 N	256 E	?	**Amsterdam**	38 S	78 E	~115?[10]	177	~3	780 / 1440
Lake Victoria(?)	3 S	36 E	?	**Hawai`i**	19 N	205 E	>100[8]	161	<26	560 / 3660
Pribilof Is.	57 N	190 E	~2[11]	**Bouvet**	54 S	3 E	≥1[6]	175	—	670 / 220
Society	18 S	211 E	~5[8]	Bayuda[1]	18 N	34 E	~4?[12]	177	~66	670 / 890
Pitcairn	26 S	230 E	~8[8]	Bazman-Taftan	28 N	61 E	≥2[13]	170	—	1000 / 890
Ewing Crater[2]	14 N	222 E	≥7-11[14]	**Comores**	12 S	43 E	≥8[15]	175	~69	1890 / 670
Samoa	14 S	187 E	~14[8]	Aïr Massif[1]	18 N	9 E	~9?[16]	176	~32	1440 / 670
Macdonald	29 S	220 E	~19[17]	Harrat as Shamad[1]	33 N	37 E	~16?[18]	175	~29	1000 / 670
Rarotonga	22 S	201 E	~1[17]	**Tibesti**	21 N	17 E	~17?[19]	176	~60	890 / 440
Kavachi	9 S	158 E	?	**Cape Verde**	16 N	335 E	~20[8]	172	~44	1330 / 1550
Juan Fernandez	34 S	278 E	>30[8]	Unnamed *(China)*	36 N	92 E	?	175	<19	890 / 1330
San Felix	26 S	280 E	>30[8]	Tengchong	25 N	98 E	≥18[20]	178	<7	890 / 560
Admiralty Is.	3 S	147 E	?	**Fernando**	4 S	328 E	≥30[8]	173	<26	1330 / 1670

Rurutu	24 S	209 E	≥10[21]	**Darfur**	13 N	24 E	~35[17]	168	~38	670 / 1110
Monowai Smt.	26 S	183 E	?	**Hoggar**	23 N	6 E	~35[17]	176	~13	1440 / 670
Socorro[1]	19 N	249 E	>25[8]	Rodrigues[1]	20 S	63 E	≤36[22]	174	<19	1330 / 780
Campbell I.	52 S	169 E	≥11[6]	**Eifel**	50 N	7 E	~40[8]	169	~31	220 / 560
Afanasy Nikitin	3 S	83 E	~80-73[23]	**Galápagos**	0 N	269 E	~90[2]	173	~9	2660 / 3000
Caroline[1]	5 N	164 E	>30[18]	**St. Helena**	8 S	346 E	~100[8]	166	~16	1670 / 1220
Easter	27 S	251 E	>100[8]	Vakak Group	34 N	68 E	?	173	<8	890 / 2110

Notes as in Table 1. Distance to next htspt, angular distance to the next hotspot listed either in Table 1 or 2 of Appendix A. The average angular deviation from exact antipodality for 29 out of 30 hotspot pairs is 6° with a standard error of ±7°. In several instances, particularly in Africa, volcanism has occurred sporadically over long time intervals at the antipodal site. In the Bayuda volcanic field of Sudan, nearly antipodal to the Society hotspot, the youngest volcanism is Pleistocene in age (~2-1 Ma). The Pleistocene volcanism was preceded by 5 other episodes ranging in age from late Cretaceous (~70 Ma) to early Pliocene (~4 Ma), each separated by long intervals of time [12]. Society hotspot volcanism has coeval ages only with the early Pliocene and younger events. Similarly, volcanism occurred at the Aïr Massif during the Oligocene to early Miocene (~35-21 Ma), and was concentrated at the intersection of structural lineaments. A second magmatic event spanned late Miocene to Pleistocene time (~9-2 Ma) [17], starting close to the initial age of the Samoan hotspot (~14 Ma). Mesozoic, early Neogene (~16 Ma), and Pliocene-to-Recent volcanic events occurred at Harrat as Shamad [19] in the eastern Mediterranean region. The nearly antipodal Macdonald hotspot has an age of ~19 Ma, and is contemporaneous with the Neogene and younger events. Older volcanic rocks exposed north of the Tibesti field have an age of ~17 Ma [20], and the young volcanoes and lava fields covering Tibesti are Quaternary in age [24]; the antipodal Rarotonga hotspot also originated during Quaternary time (~1 Ma) [17].

[1]Secondary hotspots from groupings 1-55 and 56-64 (see Table 2 in Appendix A).
[2]See Table 4 in Appendix A.

References

[1] K. Nicolaysen, F.A. Frey, K.V. Hodges, D. Weis, A. Giret, $^{40}Ar/^{39}Ar$ geochronology of flood basalts from the Kerguelen Archipelago, southern Indian Ocean: implications for Cenozoic eruption rates of the Kerguelen plume, Earth Planet. Sci. Lett. 174 (2000) 313-328.

[2] R.E. Ernst, K.L. Buchan, Large mafic magmatic events through time and links to mantle-plume heads, in: R.E. Ernst, K.L. Buchan (Eds.), Mantle Plumes: Their Identification Through Time, Geological Society of America Spec. Pap. 352, 2001, pp. 483-575.

[3] S.T. Crough, R.D. Jarrard, The Marquesas-Line Swell, J. Geophys. Res. 86 (1981) 11763-11771.

[4] S.O. Schlanger, M.O. Garcia, B.H. Keating, J.J. Naughton, W.W. Sager, J.A. Haggerty, J.A. Philpotts, R.A. Duncan, Geology and geochronology of the Line Islands, J. Geophys. Res. 89 (1984) 11261-11272.

[5] S.T. Gudlaugsson, K. Gunnarsson, M. Sand, J. Skogseid, Tectonic and volcanic events at the Jan Mayen Ridge microcontinent, in: A.C. Morton, L.M. Parson (Eds.), Early Tertiary Volcanism and the Opening of the NE Atlantic, Geol. Soc. Spec. Pub. 39, 1988, pp. 85-93.

[6] W.E. LeMasurier, J.W. Thomson (Eds.), Volcanoes of the Antarctic Plate and Southern Oceans, Am. Geophys. Union, Ant. Res. Ser. 48 (1990) 487 pp.

[7] R. Lanyon, R. Varne, A.J. Crawford, Tasmanian Tertiary basalts, the Balleny plume, and opening of the Tasman Sea (southwest Pacific Ocean), Geology 21 (1993) 555-558.

[8] B. Steinberger, Plumes in a convecting mantle: models and observations for individual hotspots, J. Geophys. Res. 105 (2000) 11127-11152.

[9] R.A. Duncan, M.A. Richards, Hotspots, mantle plumes, flood basalts, and true polar wander, Rev. Geophys. 29 (1991) 31-50.

[10] B.P. Luyendyk, W. Rennick, Tectonic history of aseismic ridges in the eastern Indian Ocean, Geol. Soc. Am. Bull. 88 (1977) 1347-1356.

[11] A. Cox, D.M. Hopkins, G.B. Dalrymple, Geomagnetic polarity epochs: Pribilof Islands, Alaska, Geol. Soc. Am. Bull. 77 (1966) 883-910.

[12] D.C. Almond, O.M. Kheir, S. Poole, Alkaline basalt volcanism in northeastern Sudan: a comparison of the Bayuda and Gedaref areas, J. Afr. Earth Sci., 2 (1984) 233-245.

[13] A. Gansser, The Taftan volcano (SE Iran), Eclogae geol. Helv. 64 (1971) 319-334.

[14] D.H. Abbott, A.A. Nunes, I.S. Leung, L. Burkle, J.T. Hagstrum, The Ewing impact structure: progress report, Eos Trans., AGU 84 (2003) F977.

[15] J. Nougier, J.M. Cantagrel, J.P. Karche, The Comores archipelago in the western Indian Ocean: volcanology, geochronology and geodynamic setting, J. African Earth Sci. 5 (1986) 135-145.

[16] M. Wilson, R. Guiraud, Late Permian to Recent magmatic activity on the African-Arabian margin of Tethys, in: D.S. Macgregor, R.T.J. Moody, D.D. Clark-Lowes (Eds.), Petroleum Geology of North Africa, Geological Society Spec. Pup. 132, 1998, pp. 231-263.

[17] V. Clouard, A. Bonneville, How many Pacific hotspots are fed by deep-mantle plumes? Geology 29 (2001) 695-698.

[18] A. Segev, Synchronous magmatic cycles during fragmentation of Gondwana: radiometric ages from the Levant and other provinces, Tectonophys. 325 (2000) 257-277.

[19] P.M. Vincent, written comm., 2003.

[20] M. Zhiguo, G.H. Curtis, L. Zhijie, T. Wei, K-Ar and strontium isotopic composition of the Tengchong volcanic rocks, west Yunnan Province, China, Geothermics 16 (1987) 283-297.

[21] C. Chauvel, W. McDonough, G. Guille, R. Maury, R. Duncan, Contrasting old and young volcanism in Rurutu Island, Austral chain, Chem. Geol. 139 (1997) 125-143.

[22] A.N. Baxter, B.G.J. Upton, W.M. White, Petrology and geochemistry of Rodrigues Island, Indian Ocean, Contrib. Mineral. Petrol. 89 (1985) 90-101.

[23] K.S. Krishna, Structure and evolution of the Afanasy Nikitin seamount, buried hills and 85°E Ridge in the northeastern Indian Ocean, Earth Planet. Sci. Lett. 209 (2003) 379-394.

[24] P.M. Vincent, The evolution of the Tibesti volcanic province, Eastern Sahara, in: T. Clifford, I.G. Glass (Eds.), African Magmatism and Tectonics, Oliver and Boyd, Edinburgh, 1970, pp. 301-319.

Appendix A. Supplementary material

Table 4

Largest well-dated impact structures (>10 km; <100 Ma [1]) and closest hotspot volcanism to their antipodes

Impact structure	Location Lat.(°)	Lon.(°)	Age (Ma)	Diam. (km)	African coord.[2] Lat.(°)	Lon.(°)	Antipodal hotspot	Location Lat.(°)	Lon.(°)	Age (Ma)	African coord.[2] Lat.(°)	Lon.(°)	Dist. (°)	Drift ($^{mm}/_{yr}$)
Structures ≥100 km in diameter with near-antipodal and near-coeval hotspots														
Chicxulub *(Mexico)*	21 N	270 E	~65	170	18 N	290 E	Christmas I.	11 S	106 E	>40[3]	5 S	112 E	167	~22
Ewing *(Pacific Ocean)*	14 N	222E	≥7-11[4]	~130	11 N	229 E	**Comores**	12 S	43 E	≥8[5]	11 S	44 E	175	~69
Popigai *(Russia)*	72 N	111 E	~36	100	76 N	127 E	Merrick Mtns.	75 S	288 E	?[6]	78 S	298 E	177	~9
Other structures with near-antipodal and near-coeval hotspots														
Montagnais *(Canada)*	43 N	296 E	~51	45	41 N	311 E	**E. Australia**	38 S	143 E	>50[7]	39 S	142 E	171	~20
Kamensk *(Russia)*	48 N	41 E	~49	25	53 N	40 E	Louisville	51 S	219 E	≥70[10]	54 S	219 E	179	~2
Haughton *(Canada)*	75 N	270 E	~23	24	73 N	277 E	Gaussberg	68 S	89 E	~20[6]	65 S	87 E	171	~43
Boltysh *(Ukraine)*	49 N	32 E	~65	24	56 N	29 E	Louisville	51 S	219 E	≥70[10]	54 S	232 E	167	~22
Structures without antipodal and coeval hotspots														
Chesapeake Bay *(USA)*	37 N	284 E	~36	90	35 N	294 E	E. Australia	38 S	143 E	>50[7]	39 S	143 E	157	~71
Kara *(Russia)*	69 N	64 E	~70	65	79 N	64 E	Mt. Waesche	67 S	179 E	≥2[6]	66 S	184 E	159	~33
Manson *(USA)*	43 N	265 E	~74	35	38 N	288 E	Amsterdam	38 S	78 E	~115[8]	23 S	80 E	152	~42
Mistastin *(Canada)*	56 N	297 E	~36	28	54 N	306 E	E. Australia	38 S	143 E	>50[7]	39 S	143 E	161	~59
Steen River *(Canada)*	60 N	242 E	~91	25	52 N	272 E	Kerguelen	49 S	69 E	~29[9]	28 S	70 E	151	~35
Ries *(Germany)*	49 N	11 E	~15	24	50 N	9 E	Antipodes Is.	50 S	179 E	≥1[6]	51 S	180 E	174	~44
Lappajärvi *(Finland)*	63 N	24 E	~73	23	69 N	11 E	Scott I.	68 S	180 E	?[6]	67 S	185 E	177	~5
Logancha *(Russia)*	66 N	96 E	~40	20	71 N	106 E	Merrick Mtns.	75 S	288 E	?[6]	78 S	298 E	172	~22
Dellen *(Sweden)*	62 N	17 E	~89	19	68 N	356 E	Scott I.	68 S	180 E	?[6]	71 S	185 E	176	~5
El'gygytgyn *(Russia)*	68 N	172 E	~4	18	68 N	173E	Bouvet I.	54 S	3 E	≥1[6]	54 S	4 E	165	—
Logoisk *(Belarus)*	54 N	28 E	~42	15	58 N	25 E	Louisville	46 S	171 E	≥70[10]	45 S	172 E	156	~63
Zhamanshin *(Kazakhstan)*	48 N	61 E	~1	14	48 N	61 E	Louisville	46 S	171 E	≥70[10]	46 S	171 E	134	—
Marquez *(USA)*	31 N	264 E	~58	13	29 N	282 E	Christmas I.	11 S	106 E	>40[3]	5 S	111 E	155	~48

Botsumtwi *(Ghana)*	7 N	359 E	~1	11	7 N	359 E	Samoa	14 S	187 E	~14[7]	14 S	187 E	169	—

See Fig. 3 in Appendix A. Most large and well-dated impact structures (14 of 21) show no apparent correlation either in near-antipodal locations or age unlike primary hotspot distribution (see Table 3 in Appendix A). African coord., location of impact structure and antipodal hotspot in coordinates of the African plate at the time of impact; Dist., angular distance between craters and hotspots in African coordinates. Other notes as in Table 2.

References

[1] Earth Impact Database (2003) [http://www.unb.ca/passc/ImpactDatabase/]

[2] I.O. Norton, Global hotspot reference frames and plate motion, in: M.A. Richards, R.G. Gordon, R.D. van der Hilst (Eds.), The History and Dynamics of Global Plate Motions, Geophysical Mono. 121, AGU, 2000, pp. 339-357.

[3] P.J. Barrett, Christmas Island (Indian Ocean) phosphate deposits, in: A.J.G. Notholt, R.P. Sheldon, D.F. Davidson (Eds.), Phosphate Deposits of the World 2, 1989, pp. 558-563.

[4] D.H. Abbott, A.A. Nunes, I.S. Leung, L. Burkle, J.T. Hagstrum, The Ewing impact structure: progress report, Eos Trans., AGU 84 (2003) F977.

[5] J. Nougier, J.M. Cantagrel, J.P. Karche, The Comores archipelago in the western Indian Ocean: volcanology, geochronology and geodynamic setting, J. African Earth Sci. 5 (1986) 135-145.

[6] W.E. LeMasurier, J.W. Thomson (Eds.), Volcanoes of the Antarctic Plate and Southern Oceans, Am. Geophys. Union, Ant. Res. Ser. 48 (1990) 487 pp.

[7] B. Steinberger, Plumes in a convecting mantle: models and observations for individual hotspots, J. Geophys. Res. 105 (2000) 11127-11152.

[8] B.P. Luyendyk, W. Rennick, Tectonic history of aseismic ridges in the eastern Indian Ocean, Geol. Soc. Am. Bull. 88 (1977) 1347-1356.

[9] K. Nicolaysen, F.A. Frey, K.V. Hodges, D. Weis, A. Giret, $^{40}Ar/^{39}Ar$ geochronology of flood basalts from the Kerguelen Archipelago, southern Indian Ocean: implications for Cenozoic eruption rates of the Kerguelen plume, Earth Planet. Sci. Lett. 174 (2000) 313-328.

[10] P. Lonsdale, Geography and history of the Louisville hotspot chain in the southwestern Pacific, J. Geophys. Res. 93 (1988) 3078-3104.

Appendix A. Supplementary material

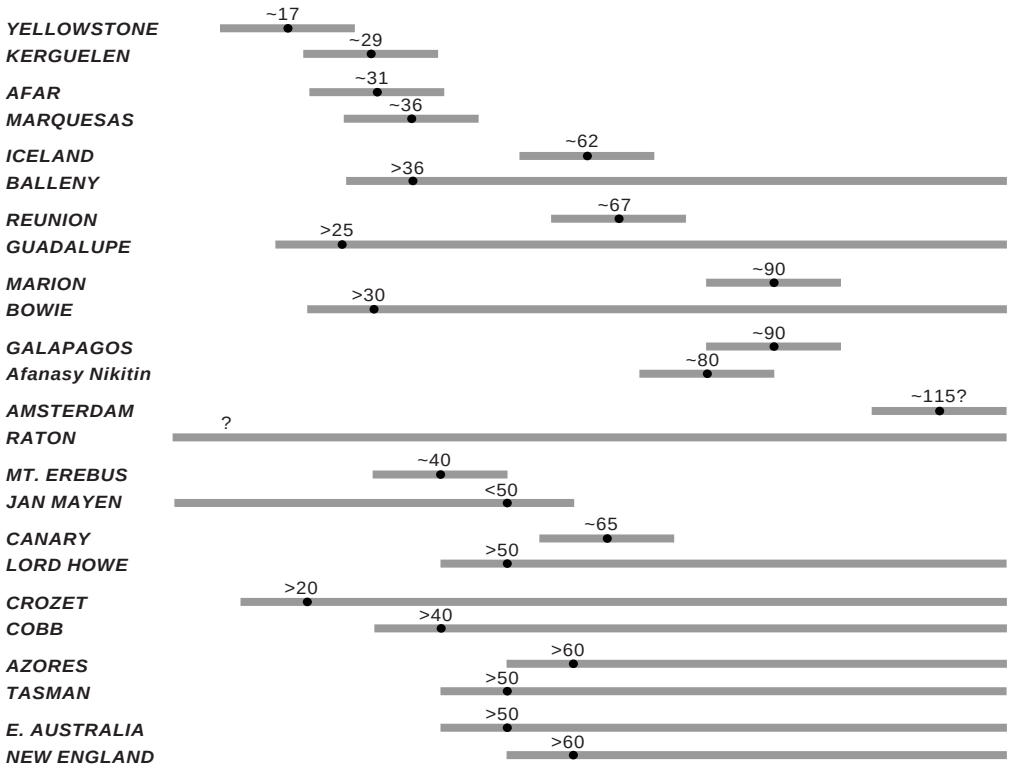

Fig. 1. Ages and age ranges (with assigned ±10 Myr error limits; see text) for the antipodal hotspots listed in Table 1.

Appendix A. Supplementary material

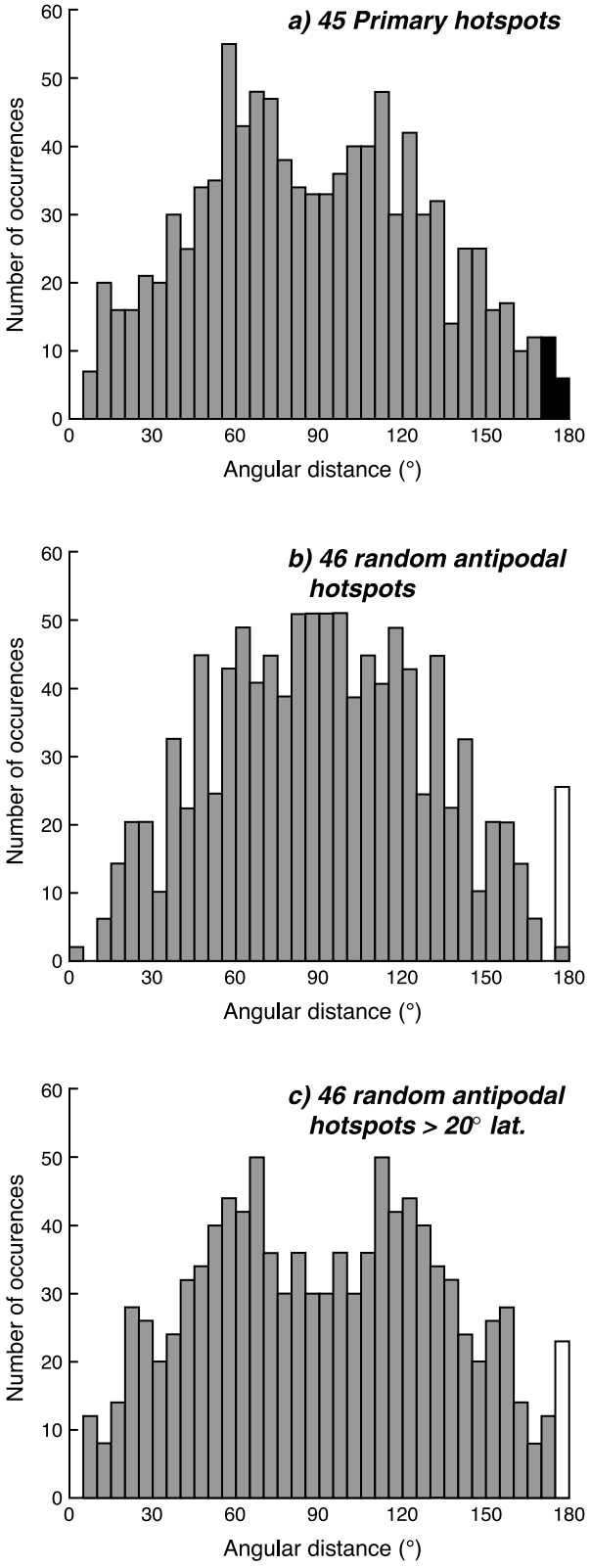

Fig. 2. Histograms of angular distances between all primary hotspots (see Table 1 in Appendix A) or artificially generated distributions of exactly antipodal hotspots plotted within 5° intervals. a) Histogram of angular distances for the 45 primary hotspots showing a local minimum at 90°. At the higher end (black columns), angular distances tend to be skewed towards 180° with 18 pairs occurring within 10° of exact antipodality. This total is greater than the number in Table 1 (11 pairs), and found statistically significant by Monte Carlo simulations (Section 3.2; Table 2), because more than one antipodal relationship for a given hotspot was accepted. b) Histogram of angular distances for 23 randomly distributed hotspots, each with an exactly antipodal hotspot, showing a more normal distribution; the histogram is symmetrical except for the 23 extra data points at 180°. c) Histogram of angular distances for 23 randomly distributed antipodal hotspot pairs as in (b) limited to an area equal to two-thirds the Earth's surface area (latitudes >20° N or S) or roughly the area of the ocean basins (see text). The histogram also shows a local minimum at 90° similar to that in (a). The actual minimum at 90° in (a), therefore, is interpreted to result from antipodal concentrations of hotspots within the Pacific Ocean and African plate (Figs. 1 and 2), along with a reduced number of hotspots in the 'equatorial' region between these two areas.

Appendix A. Supplementary material

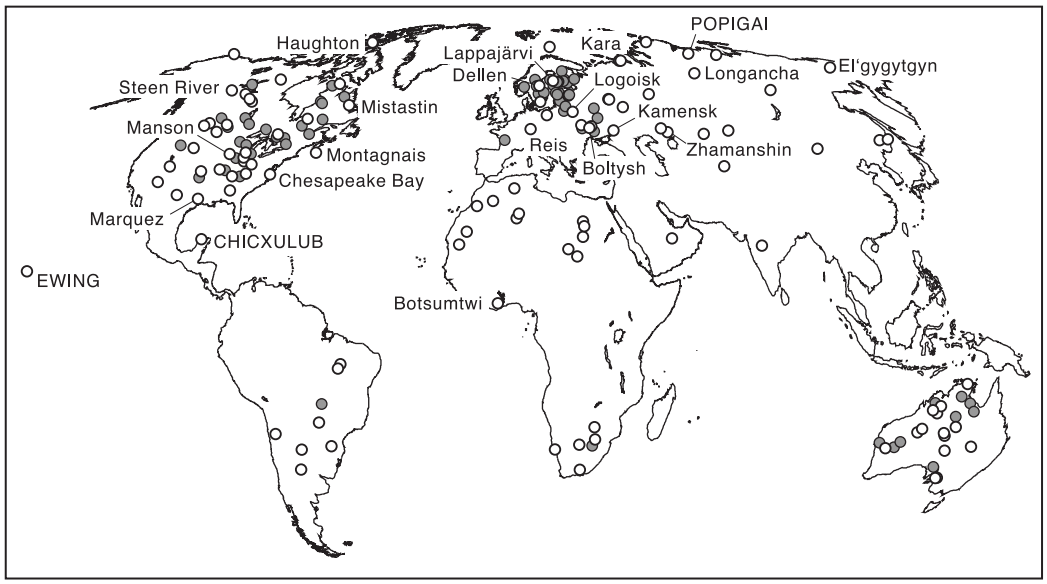

Fig. 3. World map showing locations of the 170 presently known impact structures (http://www.unb.ca/passc/ImpactDatabase/). Only the Ewing structure [53] in the eastern Pacific Ocean is on oceanic crust. Symbols for structures with ages <200 Ma are unfilled circles for comparison with the number expected on oceanic crust. The 21 largest (>10 km diameter), well-dated structures <100 Ma in age are labeled, and labels for the largest three are in capital letters (see Table 4 in Appendix A).